Optical Materials 96 (2019) 109326

Contents lists available at ScienceDirect

Optical Materials

journal homepage: www.elsevier.com/locate/optmat

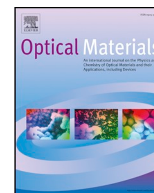

Influence of ex-situ annealing on the properties of MgF_2 thin films deposited by electron beam evaporation

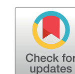

Jarno Reuna[a,*], Ville Polojärvi[a], Pertti Pääkkönen[b,1], Kimmo Lahtonen[c,2], Marianna Raappana[a], Timo Aho[a], Riku Isoaho[a], Arto Aho[a], Mika Valden[c], Mircea Guina[a]

[a] Optoelectronics Research Centre, Physics Unit, Faculty of Engineering and Natural Sciences, Tampere University, P.O. Box 692, FIN-33014, Tampere, Finland

[b] Institute of Photonics, University of Eastern Finland, P.O. Box 111, FIN-80101, Joensuu, Finland

[c] Surface Science Laboratory, Physics Unit, Faculty of Engineering and Natural Sciences, Tampere University, P.O. Box 692, FIN-33014, Tampere, Finland

ARTICLE INFO

Keywords:
Electron beam evaporation
Thin film coatings
Ellipsometry
Rapid thermal annealing (RTA)
X-ray photoelectron spectroscopy (XPS)

ABSTRACT

We report on the properties of magnesium fluoride (MgF_2) thin films deposited by electron beam evaporation as a function of substrate deposition temperature and ex-situ annealing temperature. In particular, we report on the dependence of refractive index on annealing temperature, which can be used as a tuning parameter of the optical properties. Mechanical and structural properties of the films influenced by the annealing are also examined. Changing the substrate temperature from 50 °C to 240 °C caused a decrease of the refractive index and the lowest value of 1.36 (measured at 632.8 nm) was achieved for the substrate temperature of 240 °C. Rapid thermal annealing further decreased the refractive indices to slightly below 1.32. This could indicate increase in the film porousness and removal of adsorbed water molecules. Prior annealing the film surfaces were very smooth with root mean square and mean roughness below 1 nm. Annealing above 700 °C changed the structure of the films drastically, as they started to form a granular structure, while an annealing temperature of 1000 °C increased the refractive index to a value as high as 1.5. Using X-ray photoelectron spectroscopy we show that the surface of the films consist mainly of Mg and F atoms, but also small traces of C and O are present. The Mg:F ratio remained essentially the same (43:57) between different deposition temperatures. To demonstrate the need for post-deposition annealing treatment, we have also studied the aging effect in the MgF_2 based anti-reflective coatings.

1. Introduction

MgF_2 is a widely used material for various kind of optical coatings [1–3]. Its relatively low refractive index of ~1.4 at visible wavelengths and wide transmission window from 0.11 to 4 μm [4] makes it a suitable low index material for optical coatings, such as anti-reflective coatings (ARC) and high reflectance dielectric mirrors. Multi-junction solar cells represent a specific application area where such ARCs are used, and where the specific optical properties of MgF_2 films present attractive features in terms of device performance, in particular in terms of achieving a broadband operation. To this end, thin film ARC structures utilized in multi-junction III–V semiconductor solar cells require non-absorbing high and low refractive index materials over a very broad wavelength range, extending from ultraviolet (UV) to beyond 1.5 μm, thus bringing considerable challenges for practical realization. For such coating MgF_2 is used as the low refractive index layer [2,5,6]. We should note that not just refractive index values but also the material properties are uttermost important when designing a structure that provides a low loss ARC while maintaining its functionality for a long time in varying environments. In this respect previous studies have demonstrated the effects of the deposition parameters on MgF_2 films employing electron beam evaporation [7], thermal evaporation [8,9], sputtering [10–13] and atomic layer deposition [14]. Moreover, studies focused on ion assisted deposition (IAD) showed some unwanted changes in film properties, like greater losses in the UV region and oxygen implantation [15]. It was also shown that IAD alone will not remove the need for substrate heating [16]. In this study we focus on identifying the interplay between the deposition parameters and the properties of MgF_2 thin films when employing electron beam (e-beam) evaporation. We focus in particular on the influence of the substrate temperature together with the post deposition annealing on the properties of MgF_2 with the aim to gain a good level of controllability over

* Corresponding author.
E-mail address: jarno.reuna@tuni.fi (J. Reuna).

[1] Spectroscopic ellipsometry measurements.

[2] XPS measurements.

https://doi.org/10.1016/j.optmat.2019.109326
Received 4 February 2019; Received in revised form 16 August 2019; Accepted 16 August 2019
Available online 21 August 2019
0925-3467/ © 2019 Elsevier B.V. All rights reserved.

the film properties.

2. Materials and methods

The MgF_2 thin films were deposited by a custom-built electron beam evaporator system. The device was assembled by Instrumentti Mattila Oy and it includes electron sources, crucibles, and sweep controls from Telemark Ltd and quartz monitoring from Intellemetrics Global Ltd. The system is essentially an improved bell jar vacuum chamber with two separate sections, one for materials and the electron source and another for samples. The sections are isolated with a gate valve, which enables using the upper chamber as a loading chamber. The vacuum level of the system is approximately 1×10^{-6} mbar. The films were evaporated from MgF_2 granules [17] in 16.3 cc tantalum liner. For electron beam creation we used Telemark's 7-1/2 turn tungsten filament and voltage of 8 keV with a total filament current between 4 and 8 mA. The electron beam was spiral shaped with a beam spot size approximately 3 cm^2. The evaporation rate was controlled via monitoring the filament current and the average deposition rate was kept at 0.3 nm/s. Substrate temperature (T_s) was measured from the backside of the steel substrate holder, where the holder temperature is approximated to be in thermal equilibrium with the substrate during the thin film deposition. The measurement utilized a K-type thermocouple for temperature monitoring and the heating of the substrates was done radiatively by halogen lamps.

The MgF_2 films were grown on 2" Si wafers and had a thickness of ~100 nm. The native monolayer oxide [18] on Si wafers was not removed prior to the growth and this was taken into account in spectroscopic ellipsometry measurements. Samples are identified by T_s as Ts50, Ts100, Ts150, Ts200 and Ts240, corresponding to 50 °C, 100 °C, 150 °C, 200 °C, and 240 °C, respectively. Subsequent to the growth, a test series of the samples was exposed to rapid thermal annealing (RTA) using JetFirst 100 annealing system from Jipelec Ltd. The annealing temperature T_a was varied from 300 °C to 1000 °C with 100 °C intervals. Inert N_2 atmosphere was used during temperature ramping while the annealing at the constant temperature was performed in a vacuum. Three of the annealed Ts200 samples were later characterized with atomic force microscope (AFM) and they are referred as Ts200Ta300, Ts200Ta700 and Ts200Ta900.

Film thicknesses and refractive indices of the MgF_2 layers were determined with a Rudolph AutoEL III Null ellipsometer equipped with a He/Ne laser at $\lambda = 632.8$ nm. The parameters for ellipsometric calculations were the refractive index of Si-substrate $n_S = 3.863$, substrate extinction coefficient $k_S = 0.162$ and the 70° angle of incidence. The refractive indices and film thicknesses in this study are average values of several measurements. For error limits we have used the standard deviation of single measurements, added the precision of the ellipsometer (refractive index 0.001, thickness 1 Å), and rounded up for consistent limits. For refractive index this gives an error limit of ± 0.002 and for normalized thickness an error limit of ± 0.02 a.u. with 90% level of confidence. These ellipsometric measurements were used to monitor film properties during environmental testing. The tests included measurements of the films i) as deposited, ii) after they were kept for two weeks in ambient conditions (22 °C, and relative humidity of 40%), iii) after they were soaked in water for 24 h, iv) after they were kept for a year in ambient conditions (again 22 °C and relative humidity of 40%), v) after short vacuum exposure (1 h at 1×10^{-5} mbar), and finally vi) after long vacuum exposure (3 h at 1×10^{-5} mbar and heating at 150 °C).

Spectroscopic ellipsometry was performed with a J.A.Woollam VASE spectral ellipsometer and the software used for material modelling was WVASE32® Version 3.774. All Psi and Delta ellipsometry function calculations were based on models incorporated in this software. A single oscillator Sellmeier approach was used to model the material refractive index and dispersion [19]. The uncertainty intervals for refractive indices were calculated using Sellmeier model parameter with uncertainties reported by the WVASE software. This method does not take into account the possibility of a systematic error due to the cross-dependence of the material parameters and presumption of a normal distribution for the uncertainties.

X-ray photoelectron spectroscopy (XPS) measurements were performed utilizing a non-monochromatized Al Kα X-rays (1486.6 eV) generated by DAR400 flood X-ray source (Omicron Nanotechnology GmBH) operated at 300 W for excitation of photoelectrons. The measurements were carried out in normal emission with detection area of 2.93 mm^2 (∅1.93 mm). The core level spectra were collected with a pass energy of 10 eV, producing a full width at half maximum (FWHM) of 1.09 eV for reference metallic Ag $3d_{5/2}$ peak, employing Argus hemispherical electron spectrometer (Omicron Nanotechnology GmBH) installed in a multifunctional ultra-high vacuum system with base pressure below 1×10^{-10} mbar [20].

The surface elemental concentrations and chemical states of compounds were identified by analyzing the core level photoemission spectra of C 1*s*, O 1*s*, Mg 2*p*, and F 2*s* using CasaXPS software Version 2.3.17PR1.1.2 [21]. The binding energy scale was calibrated according to the Mg 1*s* (MgF_2) component at 1305.0 eV. The spectral components were least-squares fitted with a combination of symmetric Gaussian–-Lorentzian or asymmetric Lorentzian line shapes with tail damping followed by Shirley-type background subtraction. The relative atomic concentrations were calculated using Scofield's photoionization cross sections [22] and experimentally measured transmission function of the Argus analyzer. The sampling depths of the C 1*s*, O 1*s*, Mg 2*p* (~51 eV), and F 2*s* (~30 eV) signals in MgF_2 were calculated by TPP2M formula [23] and are 8.2, 6.8, 9.4, and 9.5 nm, respectively.

Scanning electron microscope (SEM) imaging was done with a ΣIGMA™ FESEM that was operated with SmartSEM® software, both products of Carl Zeiss NTS Ltd. Acceleration voltage was 1 kV and the aperture size was 10 μm. For surface roughness measurements we used a Dimension™ 3100 AFM from Veeco Ltd and the image data was constructed with WSxM 5.0 Develop 8.2 software [24]. With these microscopic methods we obtained visual and numerical data of the structural quality of the MgF_2 films.

To test the aging performance of the e-beam evaporated MgF_2 we also designed two different ARCs for III–V multi-junction solar cells with Essential Macleod software [25] and measured the reflectance of the actual structures by using PerkinElmer Lambda 1050 spectrophotometer. The ARC structures were grown at 200 °C and did not have post-deposition RTA treatment. This T_s was chosen as a mid-value of supplier recommendations (150–250 °C) [17]. The ARC was designed for GaInP/GaAs/GaInNAsSb triple-junction solar cells with AlInP window layer [26]. The reflectance of ARCs were measured right after deposition and after exposure for a year in ambient conditions. The ARCs consisted of 103 nm MgF_2/56 nm TiO_2 and 76 nm MgF_2/39 nm Al_2O_3/50 nm TiO_2.

3. Results and discussion

In terms of optical properties, we assessed both the refractive indices and the extinction coefficients. The refractive indices measured by spectroscopic ellipsometry after deposition are plotted in Fig. 1. The measurements reveal a dependency of the refractive index on T_s, i.e. higher deposition temperature leads to a lower value of the refractive index. The decrease of refractive index as a function of fabrication temperature at selected wavelengths seems otherwise close to linear, except at the $T_s = 100$ °C. This exception could be linked to structural changes that start to take place around a substrate temperature of 100 °C.

The change of the refractive index is linked to the atomic structure of the films. MgF_2 thin films deposited by e-beam evaporation have been reported to start to crystallize at substrate temperatures above 250 °C [27] and to be partly amorphous and partly polycrystalline at temperatures below that [28]. As the densely packed amorphous

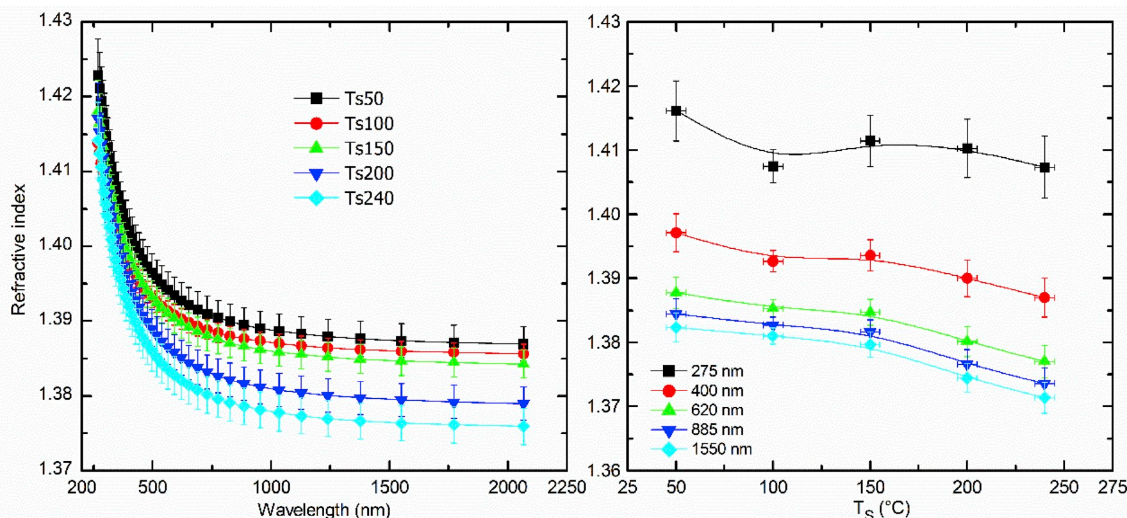

Fig. 1. Dispersion curves of the MgF_2 thin films and refractive index at selected wavelengths as a function of substrate temperature. The uncertainty bars represent 90% level of confidence.

domains start to form polycrystalline phases, they induce optically less dense structure, which lowers the refractive index. This decrease continues as a function of the deposition temperature, until the crystallization temperature (~250 °C) after which the crystalline structure starts to get denser, leading to an increase in the refractive index [9]. The results presented in Fig. 1 are in agreement with the report of Dumas et al. [28], who showed that in the range of 30 °C–150 °C the films are amorphous and in temperatures above 150 °C the films start to be polycrystalline. The results in Fig. 1 are to be taken as effective refractive indices of the films, as we later show that the film structure is porous and thus the refractive index depends also on humidity. The films are kept, however, under the same environmental conditions, so their relative comparison is sensible.

The films Ts50 and Ts240 were measured with XPS to investigate their atomic compositions and possible impurities contained in the surface structure. Fig. 2 shows the corresponding survey spectra and high resolution spectra of low binding energy region. The Mg 2*p* and F 2*s* peaks were used in the calculation of film composition because the signals are close to each other in binding energy and thus have similar sampling depth. The main transitions of Mg 1*s* and F 1*s* were also recorded and used in the chemical identification (not shown here). In the XPS scans, we detected four elements: C, O, Mg and F. The small traces of C and O indicate impurities, like hydrocarbons and water, which are adsorbed to the film surface. The low amount of the C and O impurities correspond to less than one molecular layer.

Both samples Ts50 and Ts240 showed the same Mg:F atomic ratio of 43:57, which is in good agreement with the results of Jacob et al. [29], who showed that the atomic ratio of the film surface deviates a little from the stoichiometric value of the film. Table 1 summarizes the corresponding binding energies for each element, their FWHM and relative concentrations. The binding energies and binding energy differences of Mg 1*s* (1305 eV) and F 1*s* (685.5–685.8 eV) with reference also to C 1*s* (C–C/H) correspond to Mg–F bonding, not Mg–O or metallic Mg. Besides oxidized C species, the O 1*s* peak at 534.1 eV, detected only for the sample Ts50, could be associated with water [30]. As highlighted in red in Table 1, the photoelectron peaks of Mg (1*s*, 2*s*, 2*p*) and F (1*s*, 2*s*) are narrowed with increased deposition temperature indicating increasing structural ordering and/or chemical uniformity in the MgF_2 lattice, e.g., by crystallization and removal of impurities. This is in agreement with the presumption based on the refractive index profiles in Fig. 1 and the results of Dumas et al. [28].

Fig. 3 shows the refractive index values of the MgF_2 films during environmental tests. It is expected that during the long aging periods the films have reached an equilibrium state with the environment and that the pores have been saturated with water. As the study done by Thornton and Harrison showed complete desorption of water molecules by exposing thin films to vacuum at 150 °C [31], it can expected that after the long vacuum treatment and heating, the films will no longer include significant amounts of adsorbed water molecules.

It is reasonable to expect that the porousness and thus the refractive index of the films would be directly comparable as a function of T_s. However, this is not the case right after the deposition, most likely due to partially adsorbed water during the evaporation. Ogura et al. [32] have shown that even during deposition there are some water molecules that get adsorbed to the pores of the film. As our refractive index measurements are done in ambient conditions, we are not able to calculate the actual packing density of the films, as the films already contain some amount of water. As the films age and they start to reach equilibrium with environmental conditions the order of the indices start to follow the assumptions we made based on the dispersion curves in Fig. 1. Soaking in water seems to have no effect on other samples than Ts50. This is likely to be caused by the difference in the pore size and structure, as with the smaller pore size the surface tension of water is high enough to prevent water diffusion to the pores within the used soaking time. When we compare the refractive indices of the water soaked samples to the index values of samples kept for about a year in ambient conditions, it can be concluded that the pores are not yet saturated with water due to the soaking. Furthermore, it can be seen that the short vacuum treatment is not capable of removing adsorbed water as the refractive indices still increase when compared to the values before vacuum treatment. As expected, the longer vacuum treatment with sufficient heating does remove adsorbed water from the film pores, but some hydroxyl groups are likely to remain on the surface of the film [31]. Fig. 3 shows that for the samples Ts100–Ts240 the film thickness remains rather stable as function of time. For Ts50 it would seem that after the deposition the film structure pulls together in the vertical direction of the wafer reducing the film thickness. This sort of a change in the film structure indicates relatively loose mechanical quality and high porousness.

Fig. 4 shows the surface morphology of the MgF_2 films and the cross-sectional film structure of samples Ts50 and Ts200 imaged with SEM. The images were taken after a year from the deposition.

It is clearly observable that the films deposited at temperatures below 200 °C exhibited a large amount of micro-cracks. This influences the optical and mechanical properties of the film, as the cracks offer more sites for water vapor adsorption, which in turn modifies the

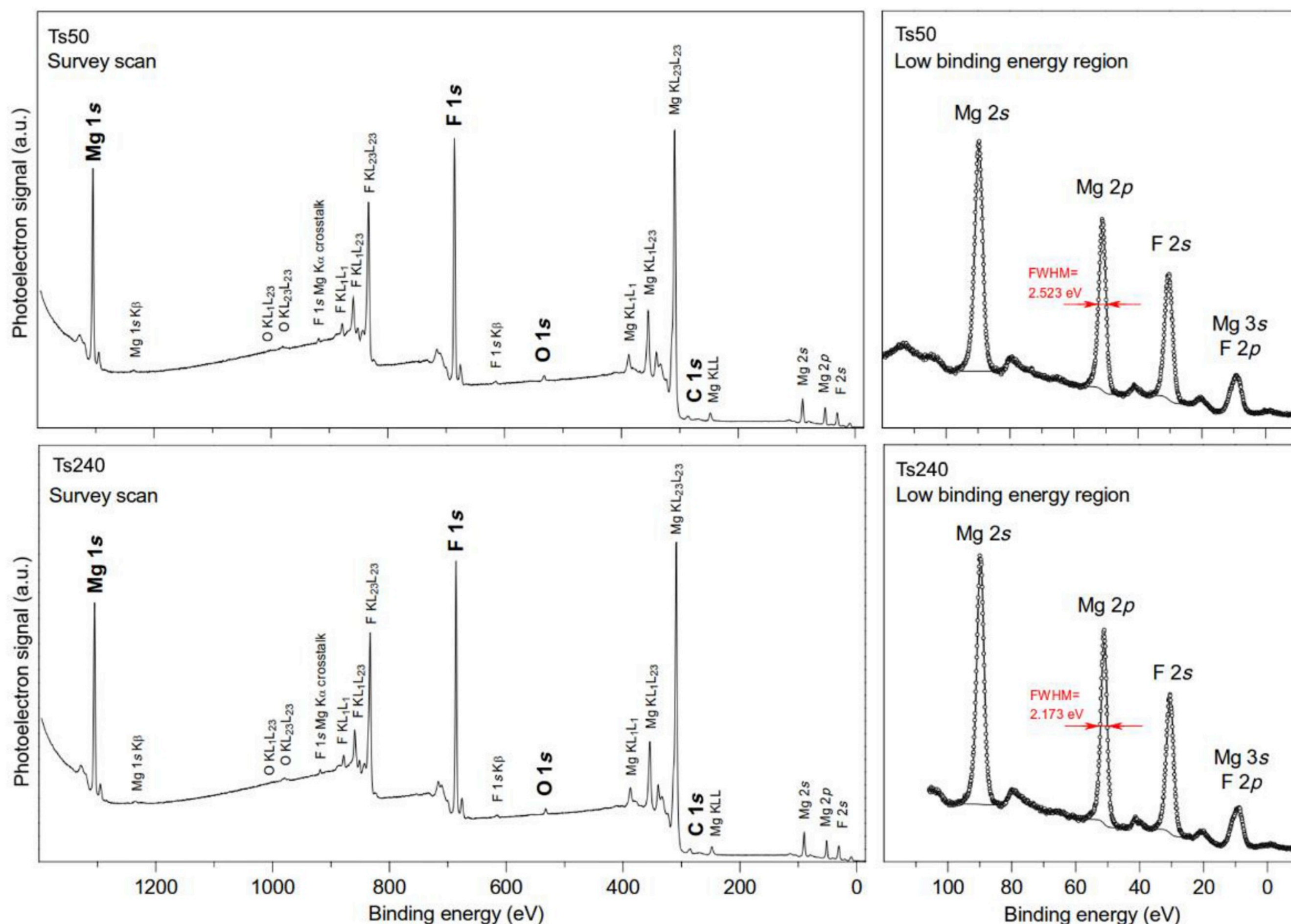

Fig. 2. XPS survey spectra (1400–0 eV) measurements and high resolution spectra (100–0 eV) of the MgF_2 thin films grown at temperatures of 50 °C and 240 °C.

effective refractive index, and decrease the abrasion resistance and the adhesion between the film and the substrate surface. Using such MgF_2 films evaporated at low temperature in multilayer structures would be problematic because micro-cracking could result in off-peeling of the coatings. In addition it seems that the cross-sectional columns of the film grown at 50 °C go through the entire film, while for the film grown at 200 °C the columns are somewhat shorter and more disorientated, thus creating a denser structure. The structural zone model (SZM) introduced by Movchan and Demchishin [33] and later revised by Thornton [34], suggests various film growth types according to the ratio of the T_s and the melting temperature of the film material T_m (both in Kelvins). For magnesium fluoride T_m is 1255 ± 3 °C [35] and the corresponding ratios of our samples are presented in Table 2.

According to the SZM, the samples Ts50, Ts100 and Ts150 belong to Zone T (ratio 0.1–0,3), which means that their structural growth is dominated by surface diffusion. This kind of growth is highly dependent of the total energy of the particles that are forming the film, which in this case is dominated by the surface temperature. Lower temperature, thus lower surface energy, leads to creation of voids in the films and increases porosity. The samples Ts200 and Ts240 belong to Zone II (ratio > 0.3), where the films have high enough energy to start to form crystalline structure.

Fig. 5 Reveals the change of refractive index as a function of T_a. When annealed below 600 °C, the refractive index of Ts200 and Ts240 remain approximately unchanged, when compared to the as deposited values. However, the samples Ts50–Ts150 exhibit significantly lower refractive index values after the RTA treatment.

This behavior is most likely due to the removal of adsorbed water, which we have assumed to originate already from the deposition. This leaves behind voids of air (n_{air} = 1.00 vs n_{water} = 1.33) and decreases the refractive index. Calculations with effective medium approximations (EMA) [37] give us the ratios of air/MgF_2 in the films, which are

Table 1
XPS results for Ts50 and Ts240 showing the corresponding binding energies for each transition (E_B), the full width at half maximum of the peaks (FWHM) and the relative atomic concentration of the elements (C_x).

Sample		C 1s		O 1s		Mg 2p	F 2s	Mg: F
		C–C/H	**C**–F X–**C**=O/–O	X–**O**(–H)	X–C=**O**/–**O** H_2**O**	**Mg**–F	Mg–**F**	
Ts50	C_x (at. %)	1.75	1.97	1.04	0.30	40.78	54.16	42.95 : 57.05
	E_B (eV)	284.78	287.37	531.81	534.14	51.00	30.28	
	FWHM (eV)	3.310	3.310	3.120	3.120	2.523	2.906	
Ts240	C_x (at. %)	2.57	1.83	1.92	–	40.27	53.41	42.99 : 57.01
	E_B (eV)	284.23	287.11	531.60		50.96	30.40	
	FWHM (eV)	2.930	2.930	3.070		2.173	2.686	

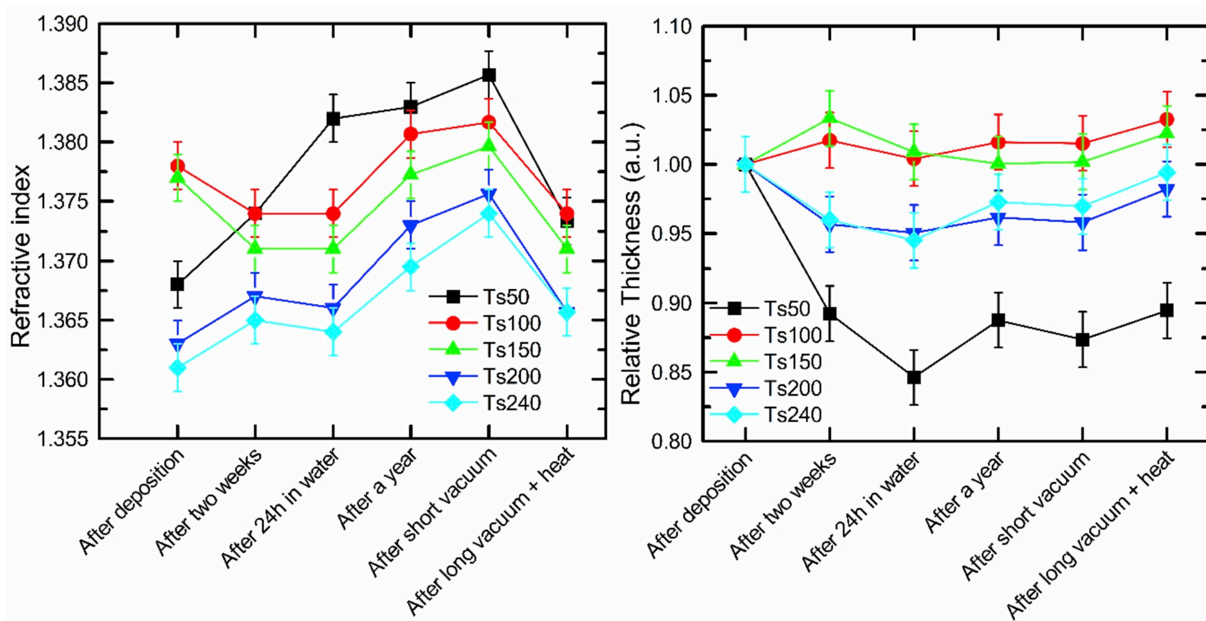

Fig. 3. Refractive indices and film thicknesses measured at λ = 632.8 nm of the MgF_2 thin films with different post deposition conditions. The uncertainty bars represent 90% level of confidence.

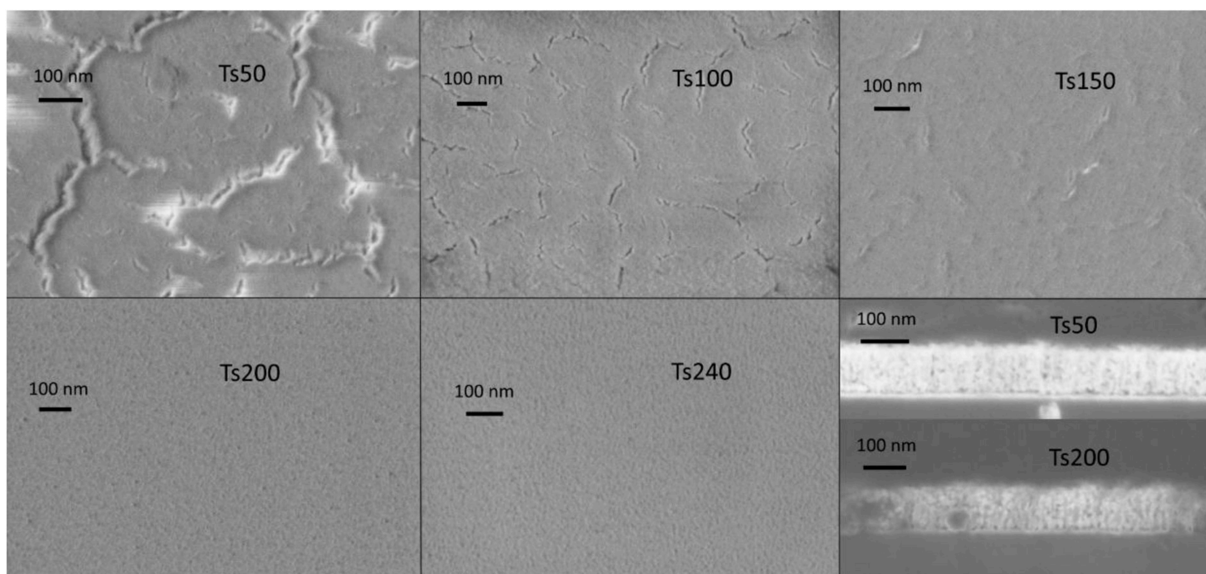

Fig. 4. Sample surfaces of the MgF_2 thin films imaged with SEM after a year exposure to ambient conditions and cross-sectional images of the samples grown in 50 °C and in 200 °C.

Table 2
Calculated structure zone model ratios T_s/T_m.

Sample	Ts50	Ts100	Ts150	Ts200	Ts240
T_s/T_m	0.21	0.24	0.28	0.31	0.34

shown in Fig. 6. The calculations are based on assumptions that

1) The pores contain only air right after the annealing procedure ($f_{MgF2} + f_{air} = 1$).
2) *The MgF_2 skeleton has a refractive index of the bulk material n = 1.378* [36].
3) The films are transparent, so the dielectric constant follows equation $\epsilon = n^2$

Here *f* stands for the volume fraction of the film material expressed in the subscript. In EMA

$$f_{MgF2}(\varepsilon_{eff} - \varepsilon_{MgF2})/(\varepsilon_{eff} + \varepsilon_{MgF2}) + f_{air}(\varepsilon_{eff} - \varepsilon_{air})/(\varepsilon_{eff} + \varepsilon_{air}) = 0, \quad (1)$$

from which we can derive

$$f_{air}/f_{MgF2} = -((\varepsilon_{eff} - \varepsilon_{MgF2})/(\varepsilon_{eff} + \varepsilon_{MgF2}))/((\varepsilon_{eff} - \varepsilon_{air})/(\varepsilon_{eff} + \varepsilon_{air})) \quad (2)$$

The value ϵ_{eff} refers now to the effective dielectric constant of the deposited film, value ϵ_{MgF2} to the bulk value and ϵ_{air} to the dielectric constant of air. Equation (2) reveals the relative amount of pores in the film and can be used to calculate the packing density *p* of the MgF_2 film, using

$$p = 1 - (f_{air}/f_{MgF2}) \quad (3)$$

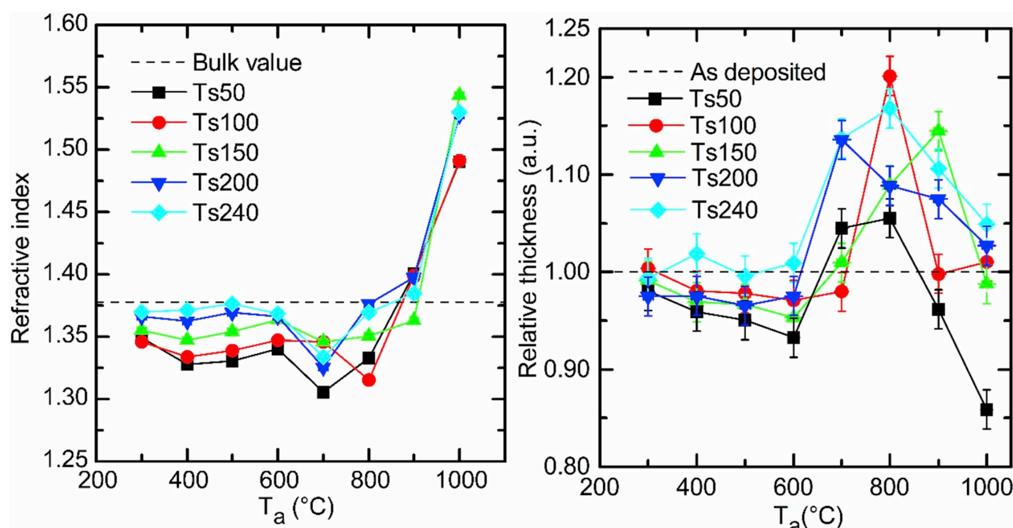

Fig. 5. Refractive indices and film thicknesses measured at λ = 632.8 nm of the MgF_2 thin films annealed in different temperatures. Bulk value by Heavens et al. [36]. The uncertainty bars represent 90% level of confidence.

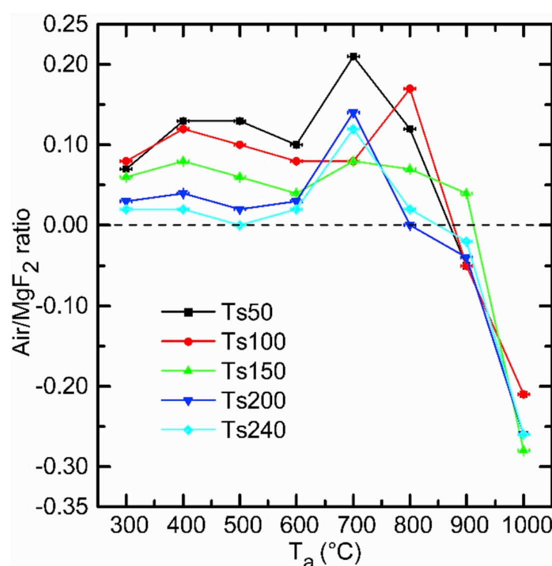

Fig. 6. Air/MgF_2 ratio of the annealed thin film samples. The uncertainty bars represent 90% level of confidence.

The air/MgF_2 ratios plotted in Fig. 6 indicate that increasing the T_a up to 600 °C improves the film quality and decreases the air content/porosity of the films, as a global minimum can be observed. At 700 °C a radical change occurs and the porosity of the films starts to increase again, after which the films seem to get denser than bulk MgF_2 based on refractive index comparison done in Fig. 5. It can also be stated that above 800 °C our assumptions for the EMA are no longer valid, which results to the negative values for air content.

As T_a increases to 700 °C the radical change of the film structure can also be seen in the film thicknesses shown in Fig. 5. The change is likely attributed to the lateral shrinkage of the films [38], which would also explain the rapid thickness increase.

As the trends of refractive index and thickness as function of T_a are very similar between samples evaporated at different T_s, we chose few annealed test pieces of the sample Ts200 for closer examination with AFM. Table 3 presents the root mean square roughness (R_{rms}) and average roughness (R_a) values measured with AFM. Surface roughness affects adhesion between thin films [39] and increases surface scattering [40], which needs to be taken into account when designing an ARC.

The surface roughness values are in good agreement with the results of Atanassov et al. [27], who studied MgF_2 films deposited by e-beam evaporation in room temperature obtaining R_{rms} of 2.276 nm and after annealing in 350 °C for 3 h R_{rms} of 14.527 nm. Our results reveal that the surface roughness increases slightly as the T_s increases, although the sample Ts150 has the lowest roughness values of the samples. This could indicate increased ordering of the lattice structure between the lower temperatures and 150 °C. Annealing further increases the surface roughness and when combined with the film thickness results of Fig. 5 a coarse surface is expected. The related surface topologies are presented in Fig. 7. It can be seen that the lowest annealing temperature does not change the surface morphology. As T_a increases, the MgF_2 films start to form granular surfaces. The sample Ts200Ta700 consists of grains with a size of roughly 50–100 nm and the sample Ts200Ta900 has a grain size of around few hundreds of nanometers.

In addition, the structural change of the annealed samples can be linked to the SZM, as has been presented by Gupta et al. [41]. According to this model, T_a/T_m ratio values between 0.25 and 0.35 correspond to the Zone T of SZM. Values higher than 0.35 can be linked to major grain growth that leads to porousness and cracking of the film. Table 4 shows the SZM ratios of the annealed samples investigated by AFM.

Based on Figs. 5 and 7 it is clear that MgF_2 films treated with RTA do not straightforwardly follow the model introduced by Gupta et al. [41]. Instead, the change from Zone T to the grain growth zone, seems to occur between 600 and 800 °C which corresponds roughly to a ratio of 0.6. The difference could be explained by shorter annealing time in our case or the overall accuracy of SZM when applied to annealed

Table 3
Surface roughness of the MgF_2 films measured by AFM.

Sample ID	Ts50	Ts100	Ts150	Ts200	Ts240	Ts200Ta300	Ts200Ta700	Ts200Ta900
R_{rms} [nm]	0.48	0.48	0.44	0.57	0.56	0.58	5.42	13.51
R_a [nm]	0.38	0.38	0.35	0.44	0.44	0.44	4.23	10.84

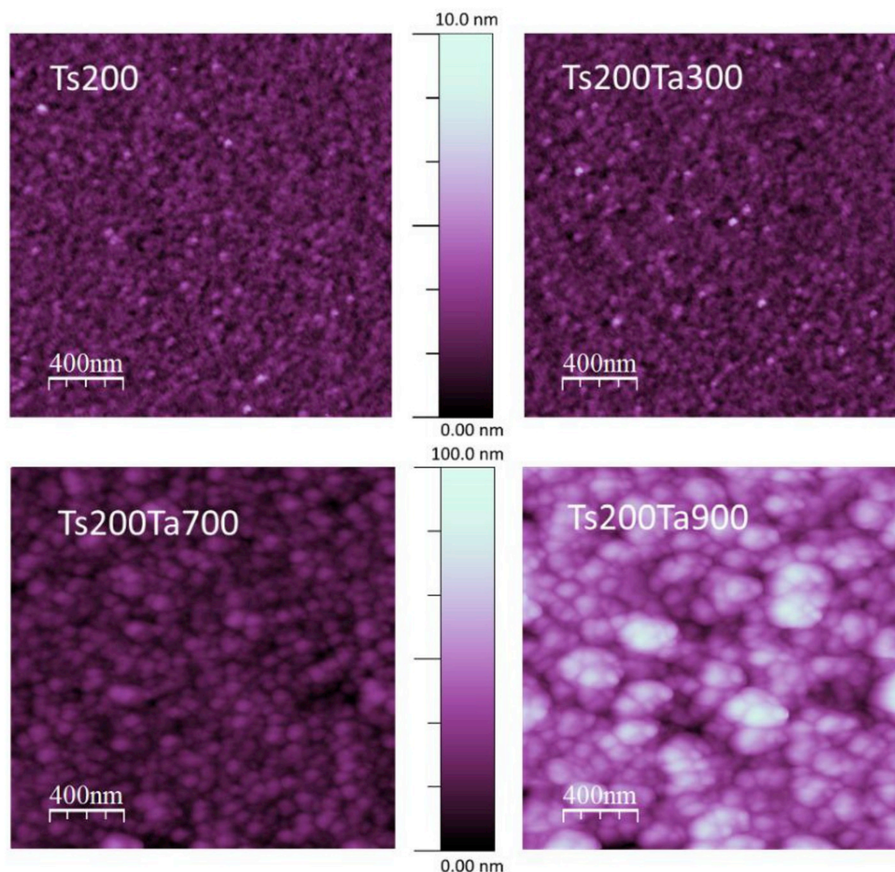

Fig. 7. Surface topology maps measured with AFM of the annealed MgF_2 thin films, initially evaporated at 200 °C and then annealed in 300 °C, 700 °C and 900 °C.

Table 4
Calculated structure zone model ratios T_a/T_m for annealed samples.

Sample	Ts200Ta300	Ts200Ta700	Ts200Ta900
T_a/T_m	0.38	0.64	0.77

samples.

The performance over time for the two test ARCs are shown in Fig. 8. It can be seen that both ARC structures decrease the average reflectance of the un-coated solar cell, roughly 30% at the visible wavelengths and then the reflectance slowly increases towards the infrared bandwidth. Ideally for multi-junction solar cells, the reflectance should remain below 5% from UV to 1.5 µm [42]. The ARCs exhibit some deterioration in their performance, as the average reflectance increases, due to prolonged exposure to ambient conditions. This is likely due to small amounts of adsorbed water. On average the absolute difference in reflectance for the double layer structure is 1.1%, while for the triple layer it is only 0.5%. The absolute reflectance difference is higher near

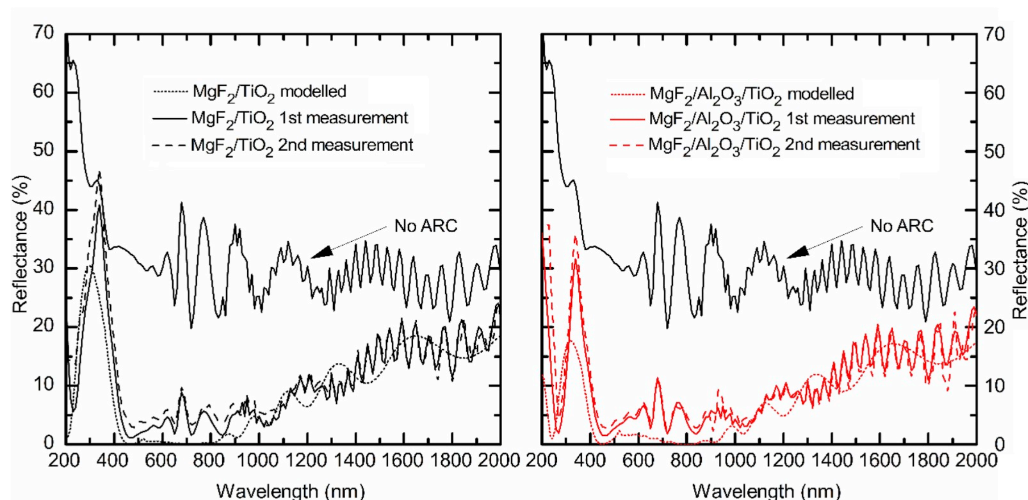

Fig. 8. Reflectance measurements of two different ARCs on a triple-junction solar cell right after deposition (1st measurement) and after a year exposure to ambient conditions (2nd measurement) and as a comparison the reflectance for the simulated design of the both ARC structures on top of the solar cell.

the UV region, and between 300 and 400 nm the values are 5.2% for the double layer structure and 3.2% for the triple layer structure.

To reach the highest efficiencies, multi-junction solar cells need to be current matched between the different junctions [43]. If the reflectance increases due time, the solar cell performance decreases, as the current balance changes [44]. Therefore the long time functionality of the coating needs to be further improved by decreasing the porousness of the MgF_2 film. This could be done by increasing the growth temperature or possibly by more effective post-growth annealing process. However, this would require also parametrization of the other layer materials to find suitable fabrication conditions for the entire ARC structure.

4. Conclusions

The properties of MgF_2 thin film structures deposited by e-beam evaporation at different substrate temperatures and subjected to post-growth annealing are reported. It was found that the growth temperature has a large impact both on the optical and structural properties without changing the Mg:F ratio of the film surface. When the T_s is increased from 50 °C to 240 °C the refractive index decreases and, on the other hand, temperatures below 200 °C lead to high porousness and micro-cracking. Due to the porosity, the film quality is more affected by humidity, which results in changes for the optical coating properties. Heating and vacuum treatment showed that the water trapping is partly a reversible process and that the films grown at higher temperature are less prone to changes in the quality due time or environmental effects. The high temperature (> 200 °C) evaporated MgF_2 films have more suitable properties for optical coatings, as they are mechanically more durable and provide a more stable refractive index that is less prone to humidity shifts.

While the films already contain small amounts of water during the deposition, the RTA process is effective in removing the water and results in improving the film quality. Excess heating, however, shrinks the films and changes their atomic structure drastically. Ellipsometric measurements suggests that the film structure can be improved at temperatures up until 600 °C. At 600 °C the porosity of the samples Ts50-Ts240 showed lowest values and no shrinkage was observed.

The functionality of MgF_2 layer for long lasting practical applications was assessed by fabricating ARCs containing MgF_2 films grown at 200 °C. The study showed that even though the mechanical quality was good, as there was no micro-cracking, the optical performance was still negatively affected by humidity. Further study would aim to test more complex multilayer designs with post-deposition RTA, to reduce the influence of humidity and long term exposure to ambient conditions. To this end, it seems beneficial to develop an effective post-deposition RTA process including the other ARC materials.

Funding

The research leading to these results has received funding from the European Research Council under the European Union's H2020 Framework [ERC-2015-AdG 695116] and Academy of Finland [Decision Number 286713]. Main author acknowledges personal support from the Fortum Foundation [201600119].

Declaration of competing interest

The authors declare that they have no known competing financial interests or personal relationships that could have appeared to influence the work reported in this paper.

References

[1] M.A. Butt, S.A. Fomchenkov, A. Ullah, P. Verma, S.N. Khonina, Biomedical band-pass filter for fluorescence microscopy imaging based on TiO 2/SiO 2 and TiO 2/MgF 2 dielectric multilayers, J. Phys. Conf. Ser. 741 (2016) 012136, , https://doi.org/10.1088/1742-6596/741/1/012136.
[2] S.E. Lee, S.W. Choi, J. Yi, Double-layer anti-reflection coating using MgF2 and CeO2 films on a crystalline silicon substrate, Thin Solid Films 376 (2000) 208–213, https://doi.org/10.1016/S0040-6090(00)01205-0.
[3] G. Kedawat, S. Srivastava, V.K. Jain, P. Kumar, V. Kataria, Y. Agrawal, B.K. Gupta, Y.K. Vijay, Fabrication of artificially stacked ultrathin ZnS/MgF2 multilayer dielectric optical filters, ACS Appl. Mater. Interfaces 5 (2013) 4872–4877, https://doi.org/10.1021/am400612q.
[4] H.K. Pulker, Characterization of optical thin films, Appl. Opt. 18 (1979) 1969, https://doi.org/10.1364/AO.18.001969.
[5] S. Liu, Y.-H. Zhang, MgF2/ZnS double-layer anti-reflection coating design for ultra-thin GaAs single-junction solar cells, Renew. Energy Environ, OSA, Washington, D.C., 2013, , https://doi.org/10.1364/OSE.2013.RM4D.5 RM4D.5.
[6] C.E. Valdivia, E. Desfonds, D. Masson, S. Fafard, A. Carlson, J. Cook, T.J. Hall, K. Hinzer, Optimization of antireflection coating design for multijunction solar cells and concentrator systems, Proc. SPIE 7099 (2008) 709910–709915, https://doi.org/10.1117/12.807675.
[7] L. Dumas, E. Quesnel, J.-Y. Robic, Y. Pauleau, Characterization of magnesium fluoride thin films deposited by direct electron beam evaporation, J. Vac. Sci. Technol. A 18 (2000) 465–469 https://doi.org/10.1116/1.582210.
[8] F. Perales, C. de las Heras, F. Agulló-Rueda, Structural properties of MgF 2 and ZnS in thin film and in multilayer optical coatings, J. Phys. D Appl. Phys. 41 (2008) 225405, , https://doi.org/10.1088/0022-3727/41/22/225405.
[9] H. Yu, H. Qi, Y. Cui, Y. Shen, J. Shao, Z. Fan, Influence of substrate temperature on properties of MgF2 coatings, Appl. Surf. Sci. 253 (2007) 6113–6117, https://doi.org/10.1016/j.apsusc.2007.01.037.
[10] J.I. Larruquert, R.A.M. Keski-Kuha, Far ultraviolet optical properties of MgF2 films deposited by ion-beam sputtering and their application as protective coatings for Al, Opt. Commun. 215 (2002) 93–99, https://doi.org/10.1016/S0030-4018(02)02229-0.
[11] J. Mashaiekhy, Z. Shafieizadeh, H. Nahidi, I. Hadi, Effect of deposition method on the optical and microstructural properties of vacuum-deposited MgF2 thin films, Optik 124 (2013) 3957–3961, https://doi.org/10.1016/j.ijleo.2013.03.018.
[12] S. Mertin, L. Marot, C.S. Sandu, R. Steiner, J.-L. Scartezzini, P. Muralt, Nanocrystalline low-refractive magnesium fluoride films deposited by reactive magnetron sputtering: optical and structural properties, Adv. Eng. Mater. 17 (2015) 1652–1659, https://doi.org/10.1002/adem.201500129.
[13] E. Quesnel, L. Dumas, D. Jacob, F. Peiró, Optical and microstructural properties of MgF2 UV coatings grown by ion beam sputtering process, J. Vac. Sci. Technol. A Vac. Surf. Films 18 (2000) 2869–2876, https://doi.org/10.1116/1.1290374.
[14] T. Pilvi, T. Hatanpaa, E. Puukilainen, K. Arstila, M. Bischoff, U. Kaiser, N. Kaiser, M. Leskela, M. Ritala, Study of a novel ALD process for depositing MgF2 thin films, J. Mater. Chem. 17 (2007) 5077–5083, https://doi.org/10.1039/B710903B.
[15] P.J. Martin, W.G. Sainty, R.P. Netterfield, D.R. McKenzie, D.J. Cockayne, S.H. Sie, O.R. Wood, H.G. Craighead, Influence of ion assistance on the optical properties of MgF(2), Appl. Opt. 26 (1987) 1235–1239, https://doi.org/10.1364/AO.26.001235.
[16] R.R. Willey, W. Optical, Improved magnesium fluoride process by ion-assisted deposition, 53rd Annu. Tech. Conf. Proc. 2010, pp. 313–319.
[17] Magnesium fluoride MgF2 for optical coating, (n.d.). https://materion.com/ResourceCenter/ProductData/InorganicChemicals/Fluorides/MagnesiumFluorideMgF2forOpticalCoating.aspx.
[18] M. Morita, T. Ohmi, E. Hasegawa, M. Kawakami, M. Ohwada, Growth of native oxide on a silicon surface, J. Appl. Phys. 68 (1990) 1272–1281, https://doi.org/10.1063/1.347181.
[19] B. Tatian, Fitting refractive-index data with the Sellmeier dispersion formula, Appl. Opt. 23 (1984) 4477, https://doi.org/10.1364/AO.23.004477.
[20] K. Lahtonen, M. Lampimäki, P. Jussila, M. Hirsimäki, M. Valden, Instrumentation and analytical methods of an x-ray photoelectron spectroscopy-scanning tunneling microscopy surface analysis system for studying nanostructured materials, Rev. Sci. Instrum. 77 (2006), https://doi.org/10.1063/1.2221539.
[21] N. Fairley, CasaXPS: Spectrum Processing Software for XPS, AES and SIMS, Version 2.3.17 PR 1.1, Casa Software Ltd., Cheshire, UK, 2009 2009 http://www.casaxps.com/.
[22] J.H. Scofield, Hartree-Slater subshell photoionization cross-sections at 1254 and 1487 eV, J. Electron. Spectrosc. Relat. Phenom. 8 (1976) 129–137, https://doi.org/10.1016/0368-2048(76)80015-1.
[23] S. Tanuma, C.J. Powell, D.R. Penn, Calculations of electron inelastic mean free paths. V. data for 14 organic compounds over the 50-2000 eV range, Surf. Interface Anal. 21 (1994) 165–176, https://doi.org/10.1002/sia.740210302.
[24] I. Horcas, R. Fernández, J.M. Gómez-Rodríguez, J. Colchero, J. Gómez-Herrero, A.M. Baro, WSXM: A software for scanning probe microscopy and a tool for nanotechnology, Rev. Sci. Instrum. 78 (2007) 1–8, https://doi.org/10.1063/1.2432410.
[25] Essential Macleod Optical Coating Design Program - User's Manual, Version 8.11, Thin Film Center Inc, 1999.
[26] Arto Aho, Dilute Nitride Multijunction Solar Cells Grown by Molecular Beam Epitaxy Julkaisu 1343 • Publication 1343 Tampere 2015 Dilute Nitride Multijunction Solar Cells Grown by Molecular Beam Epitaxy, (2015).
[27] G. Atanassov, J. Turlo, J.K. Fu, Y.S. Dai, Mechanical, optical and structural properties of TiO2 and MgF2 thin films deposited by plasma ion assisted deposition, Thin Solid Films 342 (1999) 83–92 https://doi.org/10.1016/S0040-6090(98)01407-2.
[28] L. Dumas, E. Quesnel, J.-Y. Robic, Y. Pauleau, Characterization of magnesium fluoride thin films deposited by direct electron beam evaporation, J. Vac. Sci. Technol. A Vac. Surf. Films 18 (2000) 465, https://doi.org/10.1116/1.582210.

[29] D. Jacob, F. Peiró, E. Quesnel, D. Ristau, Microstructure and composition of MgF2 optical coatings grown on Si substrate by PVD and IBS processes, Thin Solid Films 360 (2000) 133–138, https://doi.org/10.1016/S0040-6090(99)00738-5.

[30] National Institute of Standards and Technology, Gaithersburg, NIST X-Ray Photoelectron Spectroscopy Database, Version 4.1, (2012), https://doi.org/10.18434/T4T88K.

[31] E.W. Thornton, P.G. Harrison, Tin oxide surfaces. Part 1.—surface hydroxyl groups and the chemisorption of carbon dioxide and carbon monoxide on tin(IV) oxide, J. Chem. Soc., Faraday Trans. 1 Phys. Chem. Condens. Phases 71 (1975) 461, https://doi.org/10.1039/f19757100461.

[32] S. Ogura, N. Sugawara, R. Hiraga, Refractive index and packing density for MgF2 films: correlation of temperature dependence with water sorption, Thin Solid Films 30 (1975) 3–10, https://doi.org/10.1016/0040-6090(75)90298-9.

[33] A.V. Movchan, B.A. Demchishin, Structure and properties of thick condensates of nickel, titanium, tungsten, aluminum oxides, and zirconium dioxide in vacuum, Phys. Met. Metallogr. 28 (1969).

[34] J.A. Thornton, High rate thick film growth, Annu. Rev. Mater. Sci. 7 (1977) 239–260, https://doi.org/10.1146/annurev.ms.07.080177.001323.

[35] A. Duncanson, R.W.H. Stevenson, Some properties of magnesium fluoride crystallized from the melt, Proc. Phys. Soc. 72 (1958) 1001–1006, https://doi.org/10.1088/0370-1328/72/6/308.

[36] O.S. Heavens, S.D. Smith, Dielectric thin films, J. Opt. Soc. Am. 47 (1957) 469, https://doi.org/10.1364/JOSA.47.000469.

[37] V.A. Markel, Introduction to the Maxwell Garnett approximation: tutorial, J. Opt. Soc. Am. A 33 (2016) 1244, https://doi.org/10.1364/JOSAA.33.001244.

[38] D.L. Deadmore, J.S. Machin, A.W. Allen, Stability of inorganic fluorine-bearing compounds: I, binary metallic fluorides, J. Am. Ceram. Soc. 44 (1961) 105–109, https://doi.org/10.1111/j.1151-2916.1961.tb13722.x.

[39] A. Çolak, H. Wormeester, H.J.W. Zandvliet, B. Poelsema, Surface adhesion and its dependence on surface roughness and humidity measured with a flat tip, Appl. Surf. Sci. 258 (2012) 6938–6942, https://doi.org/10.1016/j.apsusc.2012.03.138.

[40] H.E. Bennett, J.O. Porteus, Relation between surface roughness and specular reflectance at normal incidence, J. Opt. Soc. Am. 51 (1961) 123, https://doi.org/10.1364/JOSA.51.000123.

[41] V. Gupta, A. Mansingh, Influence of postdeposition annealing on the structural and optical properties of sputtered zinc oxide film, J. Appl. Phys. 80 (1996) 1063–1073, https://doi.org/10.1063/1.362842.

[42] C.E. Valdivia, E. Desfonds, D. Masson, S. Fafard, A. Carlson, J. Cook, T.J. Hall, K. Hinzer, R. Vallée, M. Piché, P. Mascher, P. Cheben, D. Côté, S. LaRochelle, H.P. Schriemer, J. Albert, T. Ozaki (Eds.), Optimization of Antireflection Coating Design for Multijunction Solar Cells and Concentrator Systems, Photonics North, 2008709915, , , https://doi.org/10.1117/12.807675.

[43] W. Guter, J. Schöne, S.P. Philipps, M. Steiner, G. Siefer, A. Wekkeli, E. Welser, E. Oliva, A.W. Bett, F. Dimroth, Current-matched triple-junction solar cell reaching 41.1% conversion efficiency under concentrated sunlight, Appl. Phys. Lett. 94 (2009) 223504, , https://doi.org/10.1063/1.3148341.

[44] D.J. Aiken, Antireflection coating design for series interconnected multi-junction solar cells, Prog. Photovolt. Res. Appl. 8 (2000) 563–570, https://doi.org/10.1002/1099-159X(200011/12)8:6<563::AID-PIP327>3.0.CO;2-8.